Technical note: using Distributed Temperature Sensing for Bowen ratio evaporation measurements

Bart Schilperoort[1], Miriam Coenders-Gerrits[1], Willem Luxemburg[1], César Jiménez Rodríguez[1,3], César Cisneros Vaca[2], and Hubert Savenije[1]

[1]Delft University of Technology, Water Resources Section, Stevinweg 1, 2628 CN Delft, the Netherlands
[2]University of Twente, Faculty of Geo-Information Science and Earth Observation (ITC), Hengelosestraat 99, 7514 AE, Enschede, The Netherlands
[3]Tecnológico de Costa Rica, Escuela de Ingeniería Forestal. 159-7050, Cartago, Costa Rica

Correspondence to: Bart Schilperoort (b.schilperoort@tudelft.nl)

Abstract. Rapid improvements in the precision and spatial resolution of Distributed Temperature Sensing (DTS) technology now allow its use in hydrological and atmospheric sciences. Introduced by Euser [Hydrol. Earth Syst. Sci., 18, 2021-2032 (2014)] is the use of DTS for measuring the Bowen ratio (BR-DTS), to estimate the sensible and latent heat flux. The Bowen ratio is derived from DTS measured vertical profiles of the air temperature and wet-bulb temperature. However, in previous research the measured temperatures were not validated, and the cables were not shielded from solar radiation. Additionally, the BR-DTS method has not been tested above a forest before, where temperature gradients are small and energy storage in the air column becomes important.

In this paper the accuracy of the wet-bulb and air temperature measurements of the DTS are verified, and the resulting Bowen ratio and heat fluxes are compared to eddy covariance data. The performance of BR-DTS was tested on a 46 m high tower in a mixed forest in the centre of the Netherlands in August 2016. The average tree height is 26 to 30 m, and the temperatures are measured below, in, and above the canopy. Using the vertical temperature profiles the storage of latent and sensible heat in the air column was calculated.

We found a significant effect of solar radiation on the temperature measurements, leading to a deviation of up to 3 K. By installing screens, the error caused by sunlight is reduced to under 1 K. Wind speed seems to have a minimal effect on the measured wet-bulb temperature, both below and above the canopy. After a simple quality control, the Bowen ratio measured by DTS correlates well with eddy covariance (EC) estimates ($r^2 = 0.59$). The average energy balance closure between BR-DTS and EC is good, with a mean underestimation of 3.4 W m^{-2} by the BR-DTS method. However, during daytime the BR-DTS method overestimates the available energy, and during night-time the BR-DTS method estimates the available energy to be more negative. This difference could be related to the biomass heat storage, which is neglected in this study.

The BR-DTS method overestimates the latent heat flux on average by 18.7 W m^{-2}, with RMSE $= 90$ W m^{-2}. The sensible heat flux is underestimated on average by 10.6 W m^{-2}, with RMSE $= 76$ W m^{-2}. Estimates of the BR-DTS can be improved once the uncertainties in the energy balance are reduced. However, applying e.g. Monin-Obukhov similarity theory could provide independent estimates for the sensible heat flux. This would make the determination of the highly uncertain and difficult to determine net available energy redundant.

1 Introduction

In recent years distributed temperature sensing (DTS) technology has quickly improved (Bao and Chen, 2012). The precision and spatial resolution now allow its widespread use in hydrological and atmospheric sciences (Selker et al., 2006; Thomas et al., 2012), from measuring groundwater flow (Blume et al., 2013) and seepage into streams (Westhoff et al., 2007), to soil moisture (Steele-Dunne et al., 2010), soil heat flux (Bense et al., 2016), and wind speed (Sayde et al., 2015). First introduced by Euser et al. (2014), DTS can also be used for measuring the Bowen ratio, to estimate the evaporation flux. A dry and wet stretch of the same fibre optic cable are installed vertically to obtain the so-called dry and web bulb temperature gradient, respectively. This method mitigates some problems of the conventional Bowen ratio, since usually at least two different sensors are used to measure the temperature and vapour pressure gradients, of which each has its own independent error (Angus and Watts, 1984; Fuchs and Tanner, 1970). The DTS based Bowen ratio does not suffer from this drawback, by having a large amount of data points over the height (up to 8 per meter) with only a single sensor. It also has a resolution of 0.06 K for 1 minute averages (Silixa machine calibration), and will be more accurate when measuring over a longer time period, allowing for very small temperature gradients to be measured.

In addition to estimating the latent and sensible heat flux, the measurements can also be used to get a better understanding of the processes taking place in complex ecosystems, such as forests. A vertical temperature and humidity profile is available in high resolution and precision, both above, inside, and under the canopy. DTS can also estimate different components of the energy balance, such as the heat storage in the air column, and the soil heat flux (Jansen et al., 2011). Finally, it can be used to increase our understanding of the energy exchange between the canopy and undergrowth layers by looking at the air temperature gradient under the canopy.

This paper elaborates on the method of Euser et al. (2014), by considering more energy balance components like the latent and sensible heat storage in the air column, including a data-quality system, and using the potential air temperature. The performance of the method is tested in a mixed forest in the Netherlands by looking at the accuracy of the DTS measured air temperature and wet-bulb temperature, compared to reference temperature and humidity sensors. It appears that solar radiation can have a significant influence on the cable temperature, which can be mitigated by providing artificial shadow. Lastly the fluxes resulting from the method are compared to an eddy covariance (EC) system, and the sources of differences between the methods are shown.

2 Materials and Methods

2.1 Theory

The Bowen ratio energy balance method (BREB) combines the energy balance with the Bowen ratio (Oliphant et al., 2004). The energy balance can be described by:

$$R_N + A = \rho\lambda E + H + G_S + \frac{\mathrm{d}Q}{\mathrm{d}t} \tag{1}$$

where R_N is the net radiation (W m^{-2}), $\rho\lambda E$ the latent heat flux (W m^{-2}), H the sensible heat flux (W m^{-2}), G_S the soil heat flux (W m^{-2}), and $\frac{\mathrm{d}Q}{\mathrm{d}t}$ is the change of energy storage in the system (W m^{-2}). A represents a net advection of energy into the system (W m^{-2}), but is assumed to be 0. The energy flux associated with photosynthesis (G_P) was not measured, and is therefore not included in the equation. The Bowen ratio (β) is the ratio of the sensible heat flux to the latent heat flux and can be approximated using the air temperature gradient and the vapour pressure difference over the height (Bowen, 1926):

$$\beta = \frac{H}{\rho\lambda E} \approx \gamma \frac{\Delta T_a}{\Delta e_a} \tag{2}$$

where γ is the psychrometric constant (kPa K^{-1}) (see Eq. 10), ΔT_a the difference in air temperature between two heights (K) and Δe_a the difference in actual vapour pressure between the two heights (kPa). However, when gradients are very small, the adiabatic lapse rate can not be neglected (Barr et al., 1994). Therefore the potential temperature should be used instead:

$$\beta = \frac{H}{\rho\lambda E} = \frac{c_p}{\lambda} \frac{\partial\Theta/\partial z}{\partial q/\partial z} = \gamma \frac{\partial\Theta/\partial z}{\partial e_a/\partial z} \tag{3}$$

where c_p is the specific heat of air (MJ kg^{-1}) (See Eq. 6), λ the latent heat of vaporization (2.45 MJ kg^{-1} K^{-1}), Θ the potential temperature (K), q the specific humidity (kg kg^{-1}) (See Eq. 7) and z the height above the ground (m). The potential temperature gradient can be approximated by the right-hand side of Eq. 4, as the ratio $\frac{\Theta}{T_a}$ is nearly 1 (Pal Arya, 1988).

$$\frac{\partial\Theta}{\partial z} = \frac{\Theta}{T_a}\left(\frac{\partial T_a}{\partial z} + \Gamma\right) \approx \frac{\partial T_a}{\partial z} + \Gamma \tag{4}$$

where T_a is the air temperature (K), and Γ is the adiabatic lapse rate (typically around 0.01 K m^{-1}). The numerical implementations of Eq. 3 & 4 are explained in section 3.2 Data Processing. Under dry and unsaturated conditions the lapse rate is equal to (Pal Arya, 1988):

$$\Gamma = \frac{g}{c_p} \tag{5}$$

where g is the gravitational acceleration (9.81 m s^{-2}). The specific heat capacity of air is determined by (Stull, 2015):

$$c_p = 1.004 + 1.84q \tag{6}$$

And the specific humidity by (Pal Arya, 1988):

$$q = \varepsilon \frac{e_a}{P} \tag{7}$$

where ε is the ratio of molecular mass of water vapour to dry air (0.622), and P the atmospheric pressure (kPa). The actual vapour pressure is determined by (Allen et al., 1998):

$$e_a(T_a) = e_s(T_w) - \gamma(T_a - T_w) \tag{8}$$

where T_w is the wet-bulb temperature (K), and e_s the saturation vapour pressure (kPa) given by (Koutsoyiannis, 2012):

$$e_s(T_w) = 0.61 \cdot \exp\left(\frac{19.9 \cdot T_w}{273 + T_w}\right) \tag{9}$$

The psychrometer constant is related to the air pressure and ventilation of the psychrometer (Harrison and Wood, 2012; Allen et al., 1998). If sufficiently ventilated, the psychrometric constant is defined by (Allen et al., 1998):

$$\gamma = \frac{c_p P}{\varepsilon \lambda} = 0.665 \times 10^{-3} \cdot P \tag{10}$$

As the air pressure also varies over height, the measurements have to be corrected for elevation using the following approximation (Stull, 2015, p. 8):

$$P(z) = P_0 \cdot \exp(-z/7290) \tag{11}$$

with P_0 being the pressure at sea-level (kPa). By combining the Bowen ratio (Eq. 3) with the energy balance (Eq. 1), the latent heat flux and sensible heat flux can be determined:

$$H = \frac{R_N - G_S - \frac{\mathrm{d}Q}{\mathrm{d}t}}{1 + \frac{1}{\beta}} \tag{12}$$

$$\rho\lambda E = \frac{R_N - G_S - \frac{\mathrm{d}Q}{\mathrm{d}t}}{1 + \beta} \tag{13}$$

The storage component in the energy balance has multiple parts, ranging from the storage of heat in the soil, to the storage of heat in the form of water vapour in the air column:

$$\frac{\mathrm{d}Q}{\mathrm{d}t} = \frac{\mathrm{d}Q_H}{\mathrm{d}t} + \frac{\mathrm{d}Q_E}{\mathrm{d}t} \tag{14}$$

The changes in storage of heat and water vapour in the air column below the height at which the energy fluxes (R_N, H and $\rho\lambda E$) are measured are represented by $\frac{\mathrm{d}Q_H}{\mathrm{d}t}$ and $\frac{\mathrm{d}Q_E}{\mathrm{d}t}$ respectively (W m^{-2}). The change in biomass heat storage ($\frac{\mathrm{d}Q_B}{\mathrm{d}t}$) was not measured, and is therefore not included in this equation. $\frac{\mathrm{d}Q_H}{\mathrm{d}t}$ and $\frac{\mathrm{d}Q_E}{\mathrm{d}t}$ are defined as (Barr et al., 1994):

$$\frac{\mathrm{d}Q_H}{\mathrm{d}t} = \int_0^z \rho_a c_p \frac{\mathrm{d}T_a}{\mathrm{d}t} \mathrm{d}z \tag{15}$$

$$\frac{\mathrm{d}Q_E}{\mathrm{d}t} = \int_0^z \rho_a \lambda \frac{\mathrm{d}q}{\mathrm{d}t} \mathrm{d}z \tag{16}$$

3 Study Site

The measurements were carried out at the Speulderbos mixed forest (N: $52°15'4''$ - E: $5°41'24''$), on a tower located within a patch of Douglas Fir trees (*Pseudotsuga menziezii* (Mirb.) Franco) of 2.5 ha in Garderen, The Netherlands (Fig. 1). The surrounding area is characterized by the presence of broadleaved and coniferous tree species, distributed in blocks around the tower site (Bosveld and Bouten, 2001). Within a 500 m radius it is possible to find native tree species such as Beech (*Fagus sylvatica* L.), Pedunculate Oak (*Quercus robur* L.) and Scots Pine (*Pinus sylvestris* L.), as well as the introduced species Hemlock (*Tsuga heterophylla* (Rafinesque) Sargent) and Japanese Lark or Larch (*Larix kaempferi* (Lambert) Carriére) (Erisman et al., 1998; Raj et al., 2014; Su et al., 2009; Bosveld and Bouten, 2001; Tietema et al., 2002; Van Wijk et al., 2000; Weligepolage et al., 2013). Canopy heights differ between cover types depending on species and growing stage. Some coniferous canopies like the Douglas Fir have a canopy height between 26 m to 30 m, while the broadleaved stands can reach up to 30 m height for old growth Beech trees (Weligepolage et al., 2012; Wilkes et al., 2017), or heights under 10 m for smaller Pedunculate Oak trees.

The study site has a Oceanic Climate (Cfb) under the Köpen classification system, with a yearly average temperature of 9.8 °C and an average precipitation of 910 mm yr^{-1} (Sluijter, 2011). The topography is slightly undulating with smooth height differences (Raj et al., 2014), a well-drained soil, and a groundwater table below 40 m depth (Tiktak and Bouten, 1994). The soil texture ranges from fine sand to sandy loam (Weligepolage et al., 2012; Tietema et al., 2002; Van Wijk et al., 2000).

3.1 Setup

The temperature of fibre optic cables is measured using the DTS technique (Selker et al., 2006). In the setup, two cables with different diameters were used. The first cable has a diameter of 6 mm and has both a dry and a wetted stretch. To wet the cable it was wrapped in cloth, and water was supplied to it continuously. A second cable with a diameter of 3 mm was used to study the effects of solar radiation, as a thinner cable will warm up less (De Jong et al., 2015). However, this method added additional uncertainties due to the required extrapolation and the 3 mm cable was not used in this study. (While correlation with reference sensors improved, the uncertainty of extrapolation caused extra noise in the Bowen ratio calculations). Both cables were connected to the same DTS machine (in single-ended mode) and calibrated in a calibration bath (see Fig. 2)

The DTS machine used was the Silixa Ultima (Silixa Ltd), which has a sampling resolution of 12.5 cm, measurement resolution of 35 cm, and a measurement standard deviation of 0.06 K at a 1 minute time resolution.

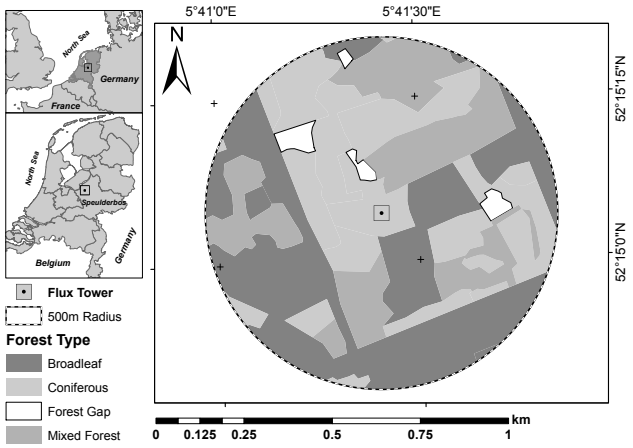

Figure 1. Forest type distribution within 500 m of the tower site at Speulderbos Forest, the Netherlands.

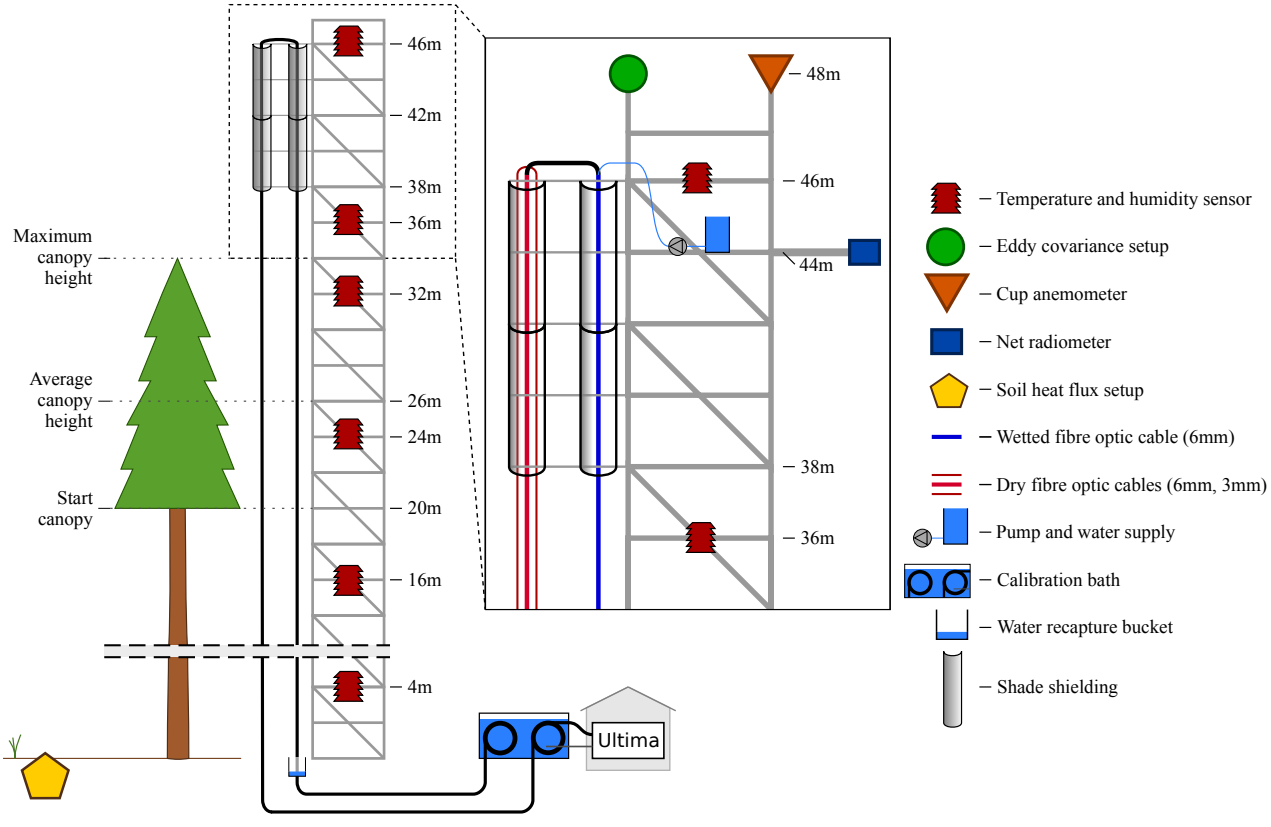

Figure 2. Schematic overview of the measurement setup at the tower.

The fibre optic cable with a diameter of 6 mm was secured at the top of the tower, with the dry stretch hanging 1.2 m away from the tower, and the wet stretch 0.25 m away. The cable with a diameter of 3 mm was secured next to the dry 6 mm cable. The response times of the cables are in the order of 2 - 3 minutes for the 6 mm cable, and 20 to 40 seconds for the 3 mm cable. The cables were secured at multiple locations distributed over the height (in and above the canopy, see Fig. 2), using loops (with a diameter of 5 cm) to prevent direct contact with the support structure. For both cables a stretch of 10 m at both the start and end was placed in a calibration bath, an enclosed Styrofoam box filled with water, along with two Pt100 temperature probes that were connected to the DTS machine. An air bubbler was installed in the Styrofoam box to ensure a homogeneous temperature distribution. The cables were shielded from direct solar radiation using screen gauze secured onto PVC rings, see Fig. 3. Only the southern 180° of the cables was shielded, to allow for sufficient ventilation. The screen gauze had holes 1.5 mm wide, and the mesh material had a diameter of 0.3 mm. Two layers of the gauze were used. Each segment of shield was 2 m long, and was secured to the tower with a horizontal beam. Due to the angle of the incident sunlight the gauze was able to block most direct sunlight, except during the early morning. To supply the wet cable with water, a reservoir was installed near the top of the tower, along with a pump. The pump speed was set to 1500 ml h^{-1} during sunny days without rainfall, and to 800 ml h^{-1} on other days, which was enough to keep the cable wet over the entire height, while keeping the influence of relatively warm water at the top of the cable at a minimum. As water supplied at the top has a higher temperature than the wet bulb temperature, the top two meters of wet cable data was excluded from the data analysis to allow the slowly flowing water to reach the wet bulb temperature.

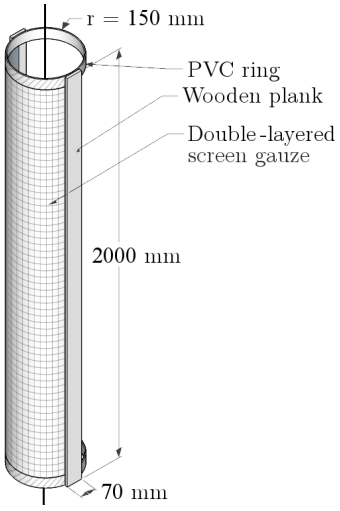

Figure 3. Schematic of one 2 m segment of the solar screen construction.

A net radiometer (Kipp & Zonen CNR4) was located on the top of the tower (48 m), measuring both incoming and outgoing short- and longwave radiation. One minute averages were logged. On the tower six humidity and temperature sensors were located over the height, at 4, 16, 24, 32, 36 and 46 meters above ground level. The lower four were Rotronic HC2-S3C03

sensors (with active ventilation), and the top two were Campbell CS216 sensors with passive ventilation. The sensors were inter-calibrated to the sensor at 24 meters. The temperature and humidity was logged at one minute averages.

At the top of the tower an eddy covariance system was installed to measure the sensible and latent heat fluxes. It consisted of a Campbell CSAT3 sonic anemometer and a Li-Cor Biosciences LI7500 gas analyser connected to a CR5000 Campbell data logger, to which the data was logged at 20 Hz.

Two cup anemometers (Onset S-WSB-M003) were used to measure the wind speed, one at the top of the tower (48 m), and one below the canopy (4 m). The data from the lower anemometer lacks the resolution to properly measure the low wind speeds below the canopy, which are at times too low to be registered. One minute average wind speeds, along with the maximum gust speeds were logged.

The biomass heat storage change and the photosynthesis energy flux were not measured. The biomass heat storage change is estimated to have a maximum of 45 W m^{-2}, and the photosynthesis energy flux is estimated to be in the order of 5 W m^{-2} (Barr et al., 1994; Michiles and Gielow, 2008). For the soil heat flux, the soil temperature was measured at different depths (1, 3, 4, 8, 20, 50 cm). Soil moisture was measured using Campbell Sci. Inc. CS616 water content reflectometers. Thermal conductivity was fitted to soil heat flux measurements done at 8 cm. The soil heat flux was then determined using the harmonics method (van der Tol, 2012).

3.2 Data Processing

The DTS machine was set to measure the cable temperature at one minute averaging intervals. For the comparison with reference temperature sensors, this one minute resolution data is used. To compare the wet-bulb temperature measured by the fibre optic cable to the reference sensors, the reference wet-bulb temperature is iteratively derived from the reference air temperature and relative humidity. For the purpose of calculating the Bowen ratio, the temperature and actual vapour pressure are averaged over time for 15 minute time periods. For DTS Bowen ratio calculations, the temperatures between 38.5 m and 44 m are used. This area is shaded from the sun by the screen gauze, and at the top of the stretch the new water on the wet cable has reached the wet-bulb temperature.

When calculating the gradients for the Bowen ratio, the 15 minute average temperature and vapour pressure are fit to the natural logarithm of the height, in the following form:

$$T_{a,\text{fit}} = a \cdot \ln(z) + b \tag{17}$$

A logarithmic shape of the profiles was assumed based on Monin-Obukhov similarity theory. A linear fit was also looked at, but it resulted in a minimal difference in the resulting fit. From the fits the temperature difference over height is then calculated:

$$\begin{aligned}\frac{\partial \Theta}{\partial z} &\approx \frac{\partial T_a}{\partial z} + \Gamma(z) \approx \frac{\Delta T_{a,\text{fit}}}{\Delta z} + \Gamma(z) \\ &\approx \frac{T_{a,\text{fit}}(z=44) - T_{a,\text{fit}}(z=38.5)}{44-38.5} + \Gamma(\bar{z}=41.25)\end{aligned} \tag{18}$$

$$\frac{\partial e_a}{\partial z} \approx \frac{\Delta e_{a,\text{fit}}}{\Delta z} = \frac{e_{a,\text{fit}}(z=44) - e_{a,\text{fit}}(z=38.5)}{44 - 38.5} \tag{19}$$

Where $\Delta T_{a,fit}$ is the difference in air temperature (K) of the fitted temperature curve, between the top and bottom of the height range used for the Bowen ratio. $\Delta e_{a,fit}$ is the difference in vapour pressure (kPa) of the fitted vapour pressure curve between those heights. Δz is the difference in height (m). The coefficients of determination of the regressions of the temperature and vapour pressure, $r_{T_a,z}$ and $r_{e_a,z}$, can be used for determining the goodness of fit. A high (positive or negative) regression means that the logarithmic slope (of the 15 minute average) is very well defined.

To calculate the air column storage terms $\frac{\mathrm{d}Q_H}{\mathrm{d}t}$ and $\frac{\mathrm{d}Q_E}{\mathrm{d}t}$ (Eq. 15 & 16), the DTS measured temperature and vapour pressure are used, except for the centre of the canopy where DTS data is not accurate due to the sunlight and lack of screens in the canopy. The temperature and specific humidity are integrated over the height from 0 to 41 m, up to the height of the Bowen ratio measurements.

As quality control scheme for the DTS-Bowen ratio, two flags are used. The first flag tests the correlation coefficient of the actual vapour pressure over height, for which we chose a lower limit of 0.20 (Eq. 20). We do not consider $r_{T_a,z}$ of the air temperature gradient as it is always higher than $r_{e_a,z}$ (as the uncertainty in e_a is higher due to the propagation of errors in T_a and T_w). The second flag is for the case where the Bowen ratio approaches -1, which causes the uncertainty in the BREB fluxes to be very high, as the denominator of Eq. 12 and Eq. 13 approaches 0 (Payero et al., 2003).

$$\text{Flag } 1 : r^2_{e_a,z} > 0.20 \tag{20}$$

$$\text{Flag } 2 : \beta < -1.1 \text{ or } \beta > -0.9 \tag{21}$$

If flag 1 is true, the outcome of the Bowen ratio calculation is considered reliable. The other datapoints are removed from further analysis. If flag 2 is also true, then the Bowen ratio can be used for calculating the atmospheric heat fluxes.

After processing the eddy covariance data using LI-COR's EddyPro® software (LI-COR Inc., 2016), several quality flags are available. The quality flag system used is from Mauder and Foken (2006), ranging from 0 (best) to 2 (worst). The eddy covariance fluxes with a quality flag of 0 or 1 are used in this research.

To summarize, the method of this paper differs in a few points from Euser et al. (2014). The fit of the Bowen ratio temperature and vapour pressure profiles is done separately, to get the correct ratio, as $\frac{\partial T}{\partial z} / \frac{\partial e_a}{\partial z} \neq \frac{\partial T}{\partial e_a}$. More energy balance storage terms are taken into account, namely the latent and specific heat storage in the air column. The potential temperature is used instead of the air temperature, to correct for the lapse rate. The local air pressure is taken into account in the calculations, as it has an influence on the psychrometric constant, specific heat capacity and specific humidity. Lastly, a system for simple quality flags is introduced to allow for simple objective quality control.

4 Results and Discussion

4.1 Meteorological Conditions

For the comparison of the DTS temperature with the reference temperature data (Section 4.2), the days 10-22 August 2016 are used.

For a good comparison between DTS and EC, both devices should work properly. Due to several technical problems with data collection, only 11 days within the measurement campaign have both eddy covariance and DTS data available, namely 10, 12-14, 19-22, and 28-30 August 2016. On the other days data is missing in either the eddy covariance or the DTS. The meteorological conditions of these days are shown in Figure 4. All days were partially clouded, or completely clouded. The wind direction was mainly west and north-east. Above the canopy the wind speed varied between 2 and 6 m s^{-1}, while under the canopy the wind speed was often too low to be measured with the cup anemometer (under 0.4 m s^{-1}).

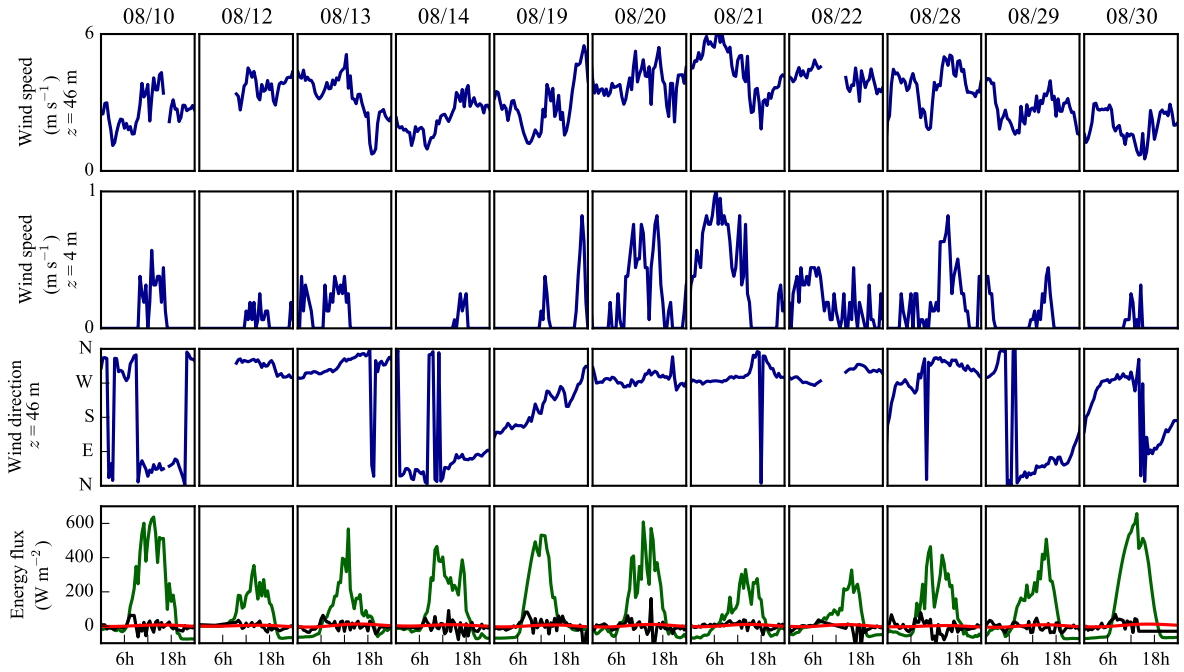

Figure 4. Meteorological conditions during the days that both DTS and eddy covariance data was available. From top to bottom: wind speed at the top of the tower, wind speed at the bottom of the tower, wind direction at the top of the tower, and the measured energy fluxes (green: net radiation, red: soil heat flux, black: energy storage change $\frac{dQ}{dt}$).

4.2 Temperature validation

In Fig. 5 the comparison between the 6 mm DTS cable and the reference sensor is shown. For the above canopy comparison, the 46 m reference sensor is compared to the cable temperatures at 44 m height, as the temperatures at the top are unreliable due to influence from the sun and the warm water from the reservoir. Below the canopy the dry cable temperature correlates perfectly with the reference sensor temperature (Fig. 5e). In and above the canopy incoming solar radiation warms up the fibre optic cable (Fig. 5a, 5c), which causes an error at 34 m where no screen was installed. This error is a deviation of up to 3 K from the reference sensor temperature (for 1 minute temperature averages). The comparison at 34 m also has an offset, this is a constant error of about 1 K, due to the reference temperature sensor drift and inter-calibration problems. The addition of screens above the canopy largely reduces the error from solar radiation to under 1 K, leading to a very good agreement between the two sensor types (Fig. 5a).

Below the canopy the wet cable temperature is in good agreement with the reference wet-bulb temperature (Fig. 5f), even though wind speeds were often low. This shows that the wet cable gives a good estimate of the wet-bulb temperature. At 34 m, where no screens were placed, the error in the wet-bulb temperature is larger than the error in the air temperature. Deviations of up to 4 K occur in the measurement period. The shielded top part of the wet cable performs much better (Fig. 5b), and errors are small (under 1 K).

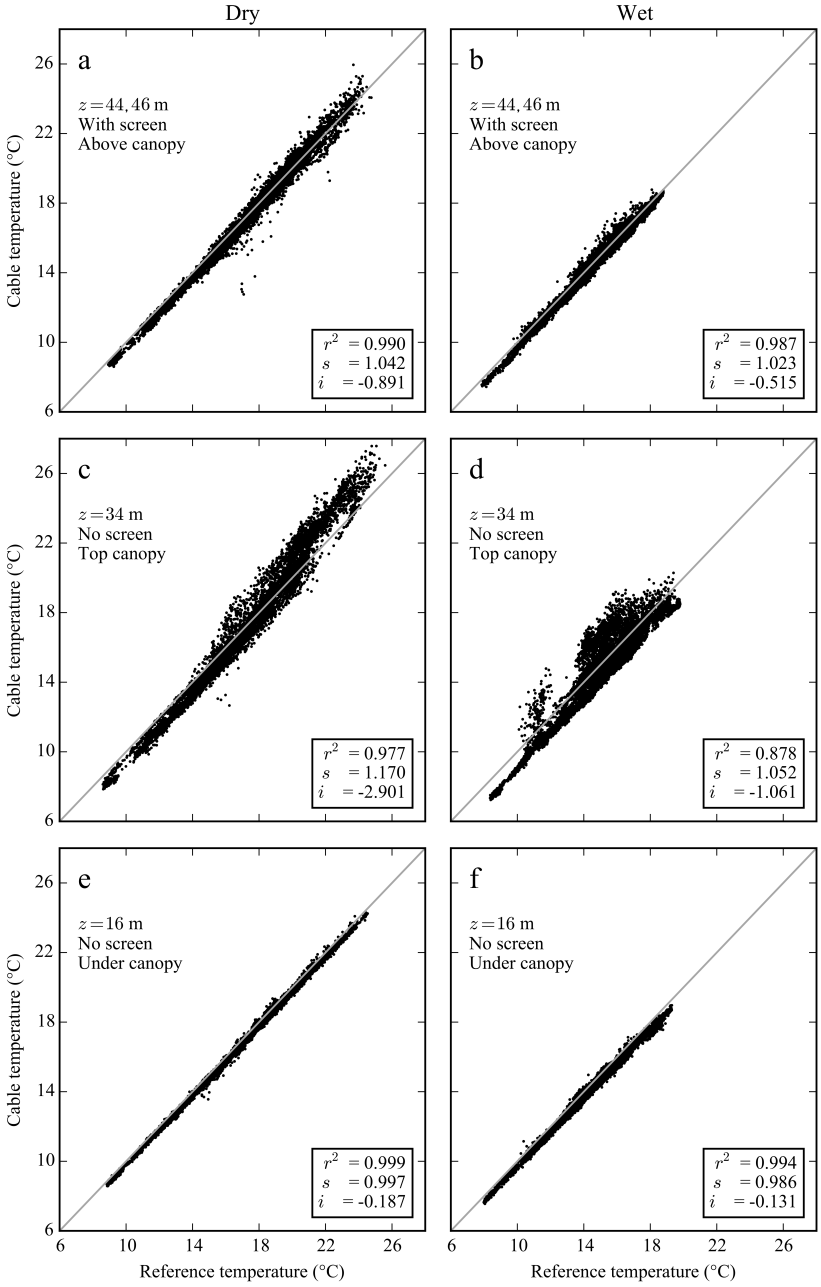

Figure 5. Comparison between the 6 mm DTS cable and reference temperatures. Grey line shows 1:1 correlation. Data from 10-23 August 2016. **a**: Dry cable at 44 m and reference air temperature at 46 m, the cable is shielded by the screen. **b**: Wet cable at 44 m and reference wet-bulb temperature at 46 m, the cable is shielded by the screen. **c**: Dry cable and reference air temperature at 34 m, the cable is exposed to direct sunlight. **d**: Wet cable and reference wet-bulb temperature at 34 m, the fibre optic cable is exposed to direct sunlight. **e**: Dry cable and reference air temperature at 16 m, under the canopy so less direct sunlight hits the fibre optic cable. **f**: Wet cable and reference wet-bulb temperature at 16 m, under the canopy so less direct sunlight hits the fibre optic cable. Shown are the linear correlation coefficients; the coefficient of determination (r^2), the slope (s), and the intercept (i).

4.3 Bowen ratio verification

The Bowen ratio resulting from the BR-DTS method (β_{DTS}) is compared to the eddy covariance Bowen ratio (β_{EC}), at a 15 minute averaging interval. In Figure 6 the correlation between the eddy covariance Bowen ratio estimate and the BR-DTS is shown. It shows a grouping around the 1:1 line, and a good correlation ($r^2 = 0.59$). The eddy covariance Bowen ratio was only calculated for fluxes with an absolute value larger than 10 W m^{-2}, as the uncertainty of the eddy covariance Bowen ratio is very high when the fluxes are small. Even the negative (night-time) values seemed to be accurate, since they passed the quality control flags. However, both eddy covariance and BR-DTS have problems measuring the night-time Bowen ratio. For eddy covariance this is due to the lower friction velocity at night (Wilson, 2002), while for the BR-DTS method the gradients are very small due to the small fluxes.

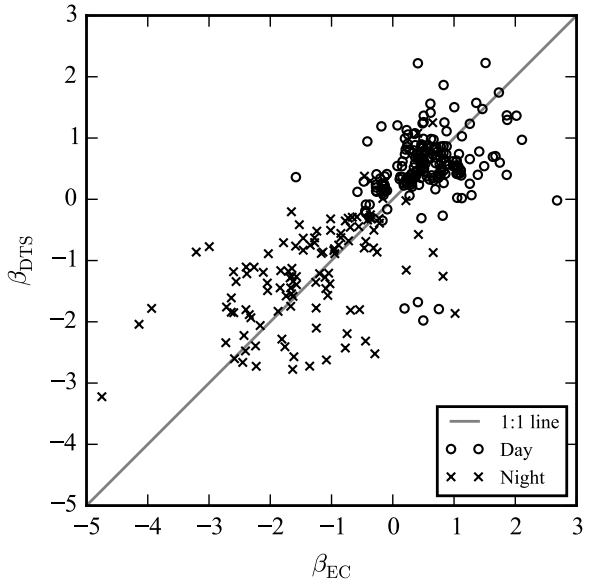

Figure 6. Correlation between the DTS measured (β_{DTS}) and eddy covariance measured (β_{EC}) Bowen ratios. Daytime data is between 7:00 and 18:00. Data from 10, 12-14, 19-22, and 28-30 August. R^2=0.59. RMSE=0.81. $n = 319$ data points.

One drawback of the DTS based Bowen ratio, is the assumption that the eddy diffusivity of heat and water vapour are the same. In reality these eddy diffusivities can be dissimilar (Irmak et al., 2014). This can cause an error (both a bias and extra noise) in the Bowen ratio as measured by the temperature and vapour pressure gradients compared to the eddy covariance Bowen ratio. Another source of differences between β_{DTS} and β_{EC}, is that the two are measured at different heights.

During the measurement period the 80% fetch of the EC system was between 200 and 300 m. By applying the findings of Stannard (1997), the Bowen ratio 80% equilibrium ratio would be reached at a fetch to height ratio of 20 to 40. This corresponds to a distance of 350 to 700 m. The fetch of the Bowen ratio will therefore not be equal to the eddy covariance fetch, which could cause some differences in measured fluxes.

4.4 Energy balance closure

A known problem in measuring fluxes is that the energy balance often does not close well. This is caused by differences in fetch between the used devices, device inaccuracies, and possibly problems with the eddy covariance method (Wilson, 2002). Part of the difference between the BR-DTS method and the eddy covariance method may be explained by this energy balance closure problem. Eddy covariance measurements have a fetch, which does not include the area close to the flux tower. The available energy in the BR-DTS method depends on measurements of net radiation, ground heat flux and heat storage change ($\frac{\mathrm{d}Q}{\mathrm{d}t}$) close to the tower. Heterogeneity in the fetch may cause differences between the two methods. In addition, the biomass heat storage change ($\frac{\mathrm{d}Q_\mathrm{B}}{\mathrm{d}t}$) was not measured for the BR-DTS method, and assumed to be 0 W m^{-2}. The photosynthesis energy flux (G_P) was also assumed to be 0 W m^{-2}.

To investigate the energy balance closure for the two methods, we summed up the available fluxes in the following equations, where $\frac{\mathrm{d}Q}{\mathrm{d}t}$ is the storage term from Eq. 14:

$$B_\mathrm{DTS} = R_N - G_S - \frac{\mathrm{d}Q}{\mathrm{d}t} \tag{22}$$

$$B_\mathrm{EC} = H_\mathrm{EC} + \rho\lambda E_\mathrm{EC} \tag{23}$$

where B_DTS is the energy available for heat fluxes in the BR-DTS method (W m^{-2}) and B_EC is the sum of the eddy covariance measured heat fluxes (W m^{-2}).

To compare the two measurement methods, a Tukey mean-difference (or Bland-Altman) plot was made (Fig. 7) (Altman and Bland, 1983). The mean of the two measurement methods is plotted against the difference between them. The mean difference (μ) between B_DTS and B_EC is a 3.4 W m^{-2} underestimation by the BR-DTS method. At low fluxes (below 100 W m^{-2}), the BR-DTS method measures less energy available for fluxes compared to eddy covariance. At high fluxes (over 400 W m^{-2}) the opposite is visible. One possible reason for this is that the biomass heat flux ($\frac{\mathrm{d}Q_\mathrm{B}}{\mathrm{d}t}$) was not measured, which causes an underestimation of the available energy in B_DTS during the night, and an overestimation during the day.

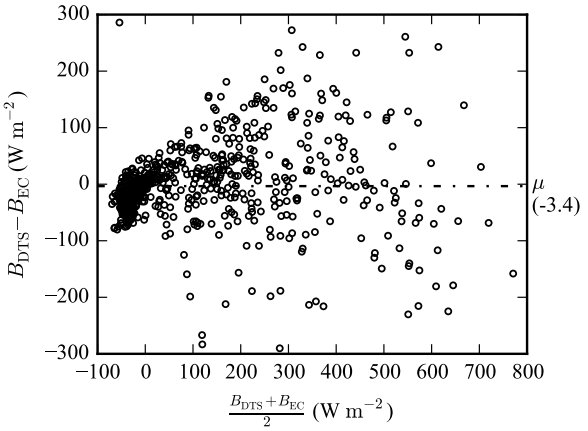

Figure 7. Tukey mean-difference plot comparing B_{DTS} and B_{EC}. With $\mu = -3.4$ W m^{-2}, RMSE $= 76$ W m^{-2}, $n = 741$ data points. (15 minute averages). Data from 10, 12-14, 19-22, and 28-30 August 2016.

4.5 Energy fluxes

Figures 8 and 9 show the mean difference plots comparing the latent and sensible heat fluxes of the eddy covariance method to the BR-DTS method. The BR-DTS fluxes are calculated above the canopy, using only temperature data from the shielded cables. The Tukey mean-difference plot for the latent heat flux shows no large bias when comparing the BR-DTS method to eddy covariance, with the mean difference being a 18.7 W m^{-2} overestimation by the BR-DTS method (Fig. 8).

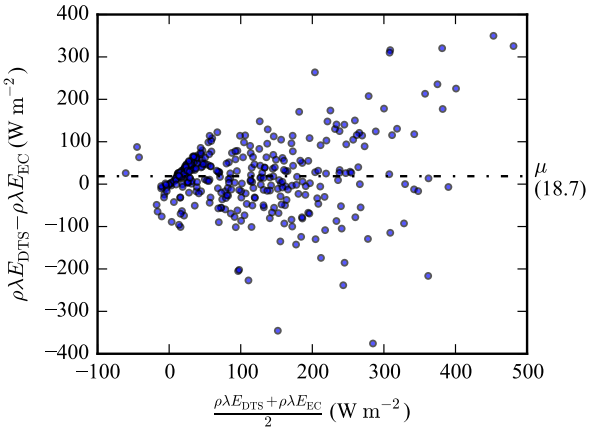

Figure 8. Tukey mean-difference plot comparing $\rho\lambda E_{\mathrm{EC}}$ and $\rho\lambda E_{\mathrm{DTS}}$. With $\mu = 18.7$ W m^{-2}, RMSE $= 90$ W m^{-2}. (15 minute averages). Data from 10, 12-14, 19-22, and 28-30 August 2016.

The Tukey mean-difference plot comparing the sensible heat flux (Fig. 9) shows a strong negative bias for negative fluxes, resulting from the negative bias in the energy balance comparison (Fig. 7). At positive fluxes there seems to be a positive bias ($H_{\mathrm{DTS}} > H_{\mathrm{EC}}$). The mean difference is small, being a 10.6 W m^{-2} underestimation by the BR-DTS method.

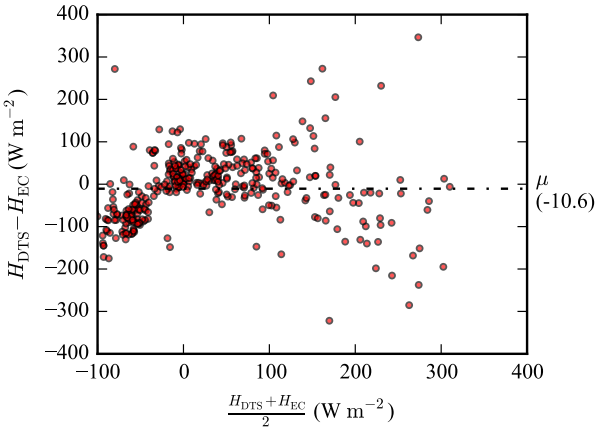

Figure 9. Tukey mean-difference plot comparing H_{EC} and H_{DTS}. With $\mu = -10.6$ W m^{-2}, RMSE $= 82$ W m^{-2}. (15 minute averages). Data from 10, 12-14, 19-22, and 28-30 August 2016.

Figure 10 shows the time series of the BR-DTS and EC measured heat fluxes. The daytime flux estimates correspond well, and follow the same trends. The night-time BR-DTS estimates of the sensible heat flux are more negative than the EC estimates, one possible reason being the energy balance differences discussed before. On many days, during the early morning and start of the evening, the BR-DTS has missing values, which is mainly due to the inversion of the gradient, as the temperature gradients changes from negative (stable conditions) to positive (unstable conditions) and vice versa. This inversion causes uncertainty, which is filtered out by the quality control flags.

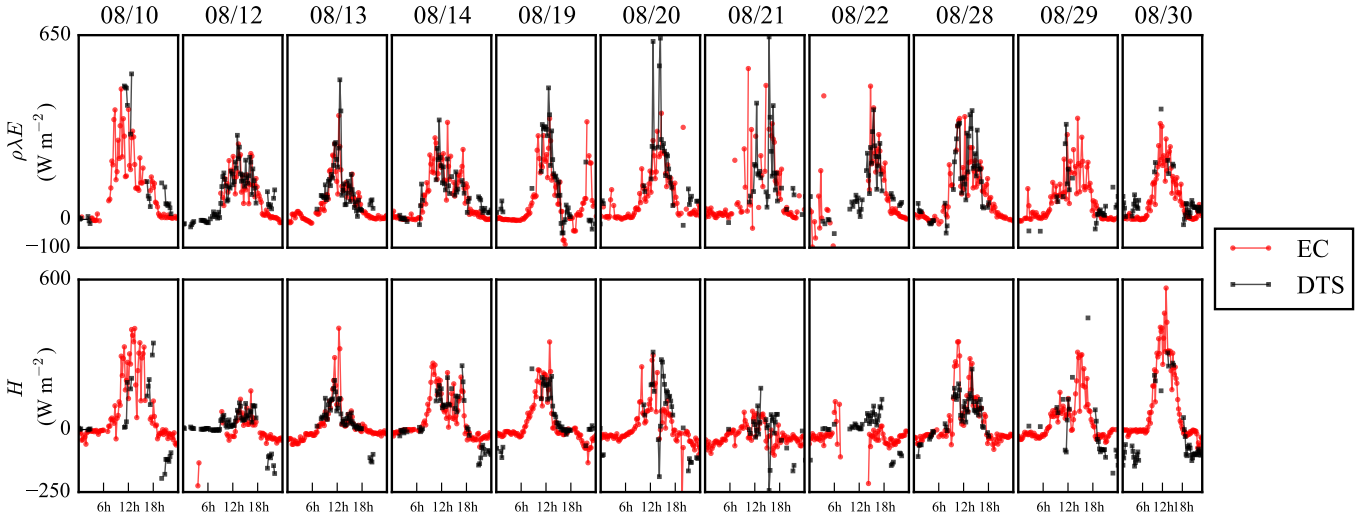

Figure 10. Plot comparing the BR-DTS and EC measured sensible (H) and latent ($\rho\lambda E$) heat fluxes over time. (15 minute averages). Data from 10, 12-14, 19-22, and 28-30 August 2016.

5 Conclusions and recommendations

This technical note investigates the use of the BR-DTS method above a forest canopy, and introduces a number of improvements on the method as presented by Euser et al. (2014). The performance is investigated by comparing the measured DTS cable temperatures to reference sensors, looking at energy balance closure, and comparing the measured Bowen ratio, sensible heat flux, and latent heat flux to eddy covariance measurements.

When comparing the fibre optic cable temperature to reference sensors, it shows that the wet-bulb and air temperatures can be well represented. Under the canopy, where the cables are shaded from direct sunlight, the DTS cable and reference sensors are in near perfect agreement. However, above the canopy direct sunlight may cause a large error, up to 3 K. This error can be largely mitigated by placing screens to block the sunlight, reducing the error to less than 1 K. Hence screens are effective and should also be placed in the canopy.

The Bowen ratio measured by DTS correlates well with eddy covariance estimates ($r^2 = 0.59$). A simple quality control method, using the goodness of fit of the vapour pressure gradient, also works well, and filters out most outliers and errors. The small gradients above the forest canopy are hard to measure accurately, which increases the uncertainty during days where fluxes (and thus gradients) are small. The Bowen ratio assumption that the eddy diffusivities of heat and vapour are equal was not studied, but can be a source of differences between the BR-DTS and eddy covariance methods. The difference in fetch for the two methods can also be a cause for differences.

The energy balance closure between the BR-DTS method and eddy covariance is in good agreement, with the mean difference being a 3.4 W m^{-2} underestimation by the BR-DTS method, and an uncertainty of RMSE $= 76$ W m^{-2}. However, the BR-DTS method estimates a more negative amount of available energy during night-time, and a more positive amount during daytime compared to eddy covariance. One cause could be the lack of biomass heat storage change measurements, which is in the order of 45 W m^{-2}. Another source for the difference is that the energy balance components of the BR-DTS method are generally point measurements, while eddy covariance and the Bowen ratio both have a large fetch. As a result, heterogeneity can cause large differences in the available energy for latent and sensible heat fluxes.

When comparing the latent heat flux of the two methods, they are in agreement, although the uncertainty is high (RMSE $= 90$ W m^{-2}). The BR-DTS method slightly overestimates the latent heat flux, with a mean difference of 18.7 W m^{-2}. The results for the sensible heat flux are similar, with an uncertainty of RMSE $= 82$ W m^{-2}, and the BR-DTS method underestimating the sensible heat flux by 10.6 W m^{-2}. However, the underestimation mainly takes place during night-time, which can be caused by differences in available energy.

While the average profiles can be useful and valuable, extra information could be gained by opting for a smaller diameter fibre optic cable, and measuring at a high frequency (1 Hz). This could give new insights into surface interactions and could show convective cells transporting heat upwards.

A way to improve the performance of the BR-DTS method is to find an independent estimate for the sensible heat flux (H), to avoid the uncertainties in the energy balance components (R_N, $\frac{\mathrm{d}Q}{\mathrm{d}t}$). Through the universal functions of the Monin-Obukhov similarity theory estimates of the sensible heat flux can be made. This could be done either by measuring the wind speed over

height (Stricker and Brutsaert, 1978) using DTS (Sayde et al., 2015), or by applying the Flux-Variance method (Katul et al., 1995). The Bowen ratio can then be used to calculate the latent heat flux.

6 Data availability

The data used in this study is available online on the 4TU data repository (Schilperoort et al., 2017).

Competing interests. The authors declare that they have no conflict of interest

Acknowledgements. This research was funded by NWO Earth and Life Sciences (ALW), veni-project 863.15.022, the Netherlands. We would like to thank M. Ucer and C. van der Tol (University of Twente) for providing us with access to their measurement location and reference data; and the students T.A. van Iersel and T. Oostdijk for assisting with setting up the DTS measurements.

References

Allen, R. G., Pereira, L. S., Raes, D., and Smith, M.: FAO Irrigation and Drainage Paper No. 56, Irrigation and Drainage, 300, 300, http://www.kimberly.uidaho.edu/water/fao56/fao56.pdf, 1998.

Altman, D. G. and Bland, J. M.: Measurement in Medicine: The Analysis of Method Comparison Studies, Journal of the Royal Statistical Society. Series D (The Statistician), 32, 307–317, doi:10.2307/2987937, 1983.

Angus, D. E. and Watts, P. J.: Evapotranspiration - How good is the Bowen ratio method?, Agricultural Water Management, 8, 133–150, doi:10.1016/0378-3774(84)90050-7, 1984.

Bao, X. and Chen, L.: Recent progress in distributed fiber optic sensors, Sensors (Basel), 12, 8601–8639, doi:10.3390/s120708601, 2012.

Barr, A. G., King, K. M., Gillespie, T. J., Den Hartog, G., and Neumann, H. H.: A comparison of bowen ratio and eddy correlation sensible and latent heat flux measurements above deciduous forest, Boundary-Layer Meteorology, 71, 21–41, doi:10.1007/BF00709218, 1994.

Bense, V., Read, T., and Verhoef, A.: Using distributed temperature sensing to monitor field scale dynamics of ground surface temperature and related substrate heat flux, Agricultural and Forest Meteorology, 220, 207–215, doi:10.1016/j.agrformet.2016.01.138, 2016.

Blume, T., Krause, S., Meinikmann, K., and Lewandowski, J.: Upscaling lacustrine groundwater discharge rates by fiber-optic distributed temperature sensing, Water Resources Research, 49, 7929–7944, doi:10.1002/2012WR013215, 2013.

Bosveld, F. and Bouten, W.: Evaluation of transpiration models with observations over a Douglas-fir forest, Agricultural and Forest Meteorology, 108, 247 – 264, doi:10.1016/S0168-1923(01)00251-9, 2001.

Bowen, I. S.: The ratio of heat losses by conduction and by evaporation from any water surface, Physical Review, 27, 779–787, doi:10.1103/PhysRev.27.779, 1926.

De Jong, S. A. P., Slingerland, J. D., and Van De Giesen, N. C.: Fiber optic distributed temperature sensing for the determination of air temperature, Atmospheric Measurement Techniques, 8, 335–339, doi:10.5194/amt-8-335-2015, 2015.

Erisman, J., Draaijers, G., Steingröver, E., Van Dijk, H., Boxman, A., and De Vries, W.: Assessment of the exposure and loads of acidifying and eutrophying pollutants and ozone, as well as their harmful influence on the vitality of the trees and the Speulder forest ecosystem as a whole, Water, Air, and Soil Pollution, 105, 539–571, 1998.

Euser, T., Luxemburg, W. M. J., Everson, C. S., Mengistu, M. G., Clulow, A. D., and Bastiaanssen, W. G. M.: A new method to measure Bowen ratios using high-resolution vertical dry and wet bulb temperature profiles, Hydrology and Earth System Sciences, 18, 2021–2032, doi:10.5194/hess-18-2021-2014, 2014.

Fuchs, M. and Tanner, C.: Error analysis of bowen ratios measured by differential psychrometry, Agricultural Meteorology, 7, 329–334, doi:10.1016/0002-1571(70)90027-0, 1970.

Harrison, R. G. and Wood, C. R.: Ventilation effects on humidity measurements in thermometer screens, Quarterly Journal of the Royal Meteorological Society, 138, 1114–1120, doi:10.1002/qj.985, 2012.

Irmak, S., Kilic, A., and Chatterjee, S.: On the Equality Assumption of Latent and Sensible Heat Energy Transfer Coefficients of the Bowen Ratio Theory for Evapotranspiration Estimations: Another Look at the Potential Causes of Inequalities, Climate, 2, 181–205, doi:10.3390/cli2030181, 2014.

Jansen, J., Stive, P. M., van de Giesen, N., Tyler, S., Steele-Dunne, S. C., and Williamson, L.: Estimating soil heat flux using Distributed Temperature Sensing, GRACE, Remote Sensing and Ground-based Methods in Multi-Scale Hydrology, pp. 140–144, 2011.

Katul, G., Goltz, S. M., Hsieh, C. I., Cheng, Y., Mowry, F., and Sigmon, J.: Estimation of surface heat and momentum fluxes using the flux-variance method above uniform and non-uniform terrain, Boundary-Layer Meteorology, 74, 237–260, doi:10.1007/BF00712120, 1995.

Koutsoyiannis, D.: Clausius-Clapeyron equation and saturation vapour pressure: simple theory reconciled with practice, European Journal of Physics, 33, 295–305, doi:10.1088/0143-0807/33/2/295, 2012.

LI-COR Inc.: EddyPro® Version 6.2 [Computer Software], 2016.

Mauder, M. and Foken, T.: Impact of post-field data processing on eddy covariance flux estimates and energy balance closure, Meteorologische Zeitschrift, 15, 597–609, doi:10.1127/0941-2948/2006/0167, 2006.

Michiles, A. A. and Gielow, R.: Above-ground thermal energy storage rates, trunk heat fluxes and surface energy balance in a central Amazonian rainforest, Agricultural and Forest Meteorology, 148, 917–930, doi:10.1016/j.agrformet.2008.01.001, 2008.

Oliphant, A. J., Grimmond, C. S. B., Zutter, H. N., Schmid, H. P., Su, H. B., Scott, S. L., Offerle, B., Randolph, J. C., and Ehman, J.: Heat storage and energy balance fluxes for a temperate deciduous forest, Agricultural and Forest Meteorology, 126, 185–201, doi:10.1016/j.agrformet.2004.07.003, 2004.

Pal Arya, S.: Introduction to Micrometeorology, Academic Press, San Diego, California, 1988.

Payero, J. O., Neale, C. M. U., Wright, J. L., and Allen, R. G.: Guidelines for validating Bowen ratio data, Transactions of the ASAE, 46, 1051, doi:10.13031/2013.13967, 2003.

Raj, R., Hamm, N. A., van der Tol, C., and Stein, A.: Variance-based sensitivity analysis of BIOME-BGC for gross and net primary production, Ecological modelling, 292, 26–36, 2014.

Sayde, C., Thomas, C. K., Wagner, J., and Selker, J.: High-resolution wind speed measurements using actively heated fiber optics, Geophysical Research Letters, 42, 10 064–10 073, doi:10.1002/2015GL066729, 2015.

Schilperoort, B., Cisneros Vaca, C. R., and Jiménez Rodríguez, C. D.: Speulderbos flux, storage, and temperature profile measurements, doi:10.4121/uuid:5c81f10a-1249-4b85-8dec-2b029dd88b99, 2017.

Selker, J. S., Thévenaz, L., Huwald, H., Mallet, A., Luxemburg, W., Van De Giesen, N., Stejskal, M., Zeman, J., Westhoff, M., and Parlange, M. B.: Distributed fiber-optic temperature sensing for hydrologic systems, Water Resources Research, 42, 1–8, doi:10.1029/2006WR005326, 2006.

Silixa Ltd: ULTIMA™ DTS, http://silixa.com/technology/ultima-dts/, visited on 2017-06-26.

Sluijter, R.: De Bosatlas van het klimaat, Noordhoff Uitgevers, Groningen, 2011.

Stannard, D. I.: A Theoretically Based Determination of Bowen-ratio Fetch Requirements, Boundary-Layer Meteorology, 83, 375–406, doi:10.1023/A:1000286829849, https://doi.org/10.1023/A:1000286829849, 1997.

Steele-Dunne, S. C., Rutten, M. M., Krzeminska, D. M., Hausner, M., Tyler, S. W., Selker, J., Bogaard, T. A., and Van De Giesen, N. C.: Feasibility of soil moisture estimation using passive distributed temperature sensing, Water Resources Research, 46, 1–12, doi:10.1029/2009WR008272, 2010.

Stricker, H. and Brutsaert, W.: Actual evapotranspiration over a summer period in the "Hupsel catchment", Journal of Hydrology, 39, 139–157, doi:10.1016/0022-1694(78)90119-1, 1978.

Stull, R.: Practical Meteorology - An Algebra-based Survey of Atmospheric Science, Department of Earth, Ocean & Atmospheric Sciences, University of British Columbia, Vancouver, BC, doi:10.14288/1.0300441, 2015.

Su, Z., Timmermans, W., Van der Tol, C., Dost, R., Bianchi, R., Gómez, J., House, A., Hajnsek, I., Menenti, M., Magliulo, V., et al.: EAGLE 2006-Multi-purpose, multi-angle and multi-sensor in-situ and airborne campaigns over grassland and forest, Hydrology and earth system sciences, 13, 833, 2009.

Thomas, C. K., Kennedy, A. M., Selker, J. S., Moretti, A., Schroth, M. H., Smoot, A. R., Tufillaro, N. B., and Zeeman, M. J.: High-Resolution Fibre-Optic Temperature Sensing: A New Tool to Study the Two-Dimensional Structure of Atmospheric Surface-Layer Flow, Boundary-Layer Meteorology, 142, 177–192, doi:10.1007/s10546-011-9672-7, 2012.

Tietema, A., Mol-Dijkstra, J., Kros, J., Vries, W., et al.: Dynamic nitrogen deposition thresholds during forest stand development in a Douglas fir forest analysed with two nitrogen models SMART2 and MERLIN, Hydrology and Earth System Sciences, 6, 375–382, 2002.

Tiktak, A. and Bouten, W.: Soil water dynamics and long-term water balances of a Douglas fir stand in the Netherlands, Journal of Hydrology, 156, 265–283, 1994.

van der Tol, C.: Validation of remote sensing of bare soil ground heat flux, Remote Sensing of Environment, 121, 275–286, doi:10.1016/j.rse.2012.02.009, 2012.

Van Wijk, M., Dekker, S., Bouten, W., Bosveld, F., Kohsiek, W., Kramer, K., and Mohren, G.: Modeling daily gas exchange of a Douglas-fir forest: comparison of three stomatal conductance models with and without a soil water stress function, Tree Physiology, 20, 115–122, 2000.

Weligepolage, K., Gieske, A., and Su, Z.: Surface roughness analysis of a conifer forest canopy with airborne and terrestrial laser scanning techniques, International Journal of Applied Earth Observation and Geoinformation, 14, 192 – 203, doi:10.1016/j.jag.2011.08.014, 2012.

Weligepolage, K., Gieske, A., and Su, Z.: Effect of spatial resolution on estimating surface albedo: A case study in Speulderbos forest in The Netherlands, International Journal of Applied Earth Observation and Geoinformation, 23, 18–28, 2013.

Westhoff, M. C., Savenije, H. H. G., Luxemburg, W. M. J. ., Stelling, G. S., van de Giesen, N. C., Selker, J. S., Pfister, L., and Uhlenbrook, S.: A distributed stream temperature model using high resolution temperature observations, Hydrology and Earth System Sciences, 11, 1469–1480, doi:10.5194/hess-11-1469-2007, 2007.

Wilkes, P., Lau, A., Disney, M., Calders, K., Burt, A., de Tanago, J. G., Bartholomeus, H., Brede, B., and Herold, M.: Data acquisition considerations for Terrestrial Laser Scanning of forest plots, Remote Sensing of Environment, 196, 140 – 153, doi:10.1016/j.rse.2017.04.030, 2017.

Wilson, K.: Energy balance closure at FLUXNET sites, Agricultural and Forest Meteorology, 113, 223–243, doi:10.1016/S0168-1923(02)00109-0, 2002.